Modelling and Simulation of a PV-Driven Refrigerator with Phase Change Materials in the Internal Walls

Adriana Coca-Ortegón[1], Victor Torres-Toledo[2], Joachim Müller[2], Alberto Coronas[1]

[1]Universitat Rovira i Virgili, Department of Mechanical Engineering, Tarragona (Spain)

[2] Universität Hohenheim, Agricultural Engineering Institute, Stuttgart (Germany)

Abstract

Refrigeration systems driven by photovoltaic energy are a useful solution for those regions of developing countries in which there is no electrical supply, or this supply is unreliable. These systems usually store energy through use of electrical lead-acid batteries. However, other energy storage options, with lower environmental effects, such us thermal energy storage, can be applied.

This study presents a model and simulation of a horizontal direct-current, compression refrigerator, which is driven by a photovoltaic sub-system. The system has latent thermal energy storage, through the incorporation of a slab with phase-change materials, next to the evaporator-wall, inside the refrigerator.

System performance was analysed with a product temperature of 11ºC, and includes three materials. One was water, and the others were phase-change materials, with average melting temperatures of 5°C and 9°C, respectively. Results indicate that the lead-acid battery capacity in such a PV-driven refrigerator can be reduced between 16% and 78%, in accordance with system operating conditions and the phase change material selected for the studied application.

Keywords: PV- refrigerator, thermal energy storage, phase change materials.

1. Introduction

Compression refrigeration systems driven by Photovoltaic (PV) energy are a useful alternative for those regions of developing countries in which there is no electrical supply, or there are frequent electrical outages (Pedersen and Katic, 2016). This type of systems usually store energy through electric lead-acid batteries. However, alternative energy storage options, with lower environmental effects, can also be applied. These options include Thermal Energy Storage (TES), based on Phase Change Materials (PCMs).

Main environmental effects of electrical batteries are related to the toxicity of the substances they content, like lead and sulphuric acid, which can be harmful to water, land and human health, and imply high costs of handling and recycling processes (Schaddelee-Scholten and Tempowski, 2017; Sørensen, 2015). On the other hand, thermal energy storage based on PCMs, for cold applications, use materials such as hydrated salts and paraffin (Oró et al., 2012), without any toxic substances and lower environmental effects.

PCM integration in refrigerators has been analysed in several studies throughout the past decade (Azzouz et al., 2009; Cheng et al., 2017; Marques et al., 2014). Generally, PCMs have been installed in contact with the evaporator surface or with the condenser. The most relevant effects pointed out in these studies are: 1) An increase in compressor cycle time, 2) higher product temperature stability, and 3) A decrease in electrical consumption for single speed compressors, owing to lower compressor starts during global system operation.

Despite these reported studies, there are still few focused on PCM integration into PV-refrigerators. In order to fulfil this gap, this study presents a model and simulation of a horizontal PV-refrigerator, which includes latent thermal storage, by incorporating a TES slab, in contact to the evaporator wall. A case was analysed, in which the product temperature was 11ºC, and the simulation included three different materials, one was water, and the other two were PCMs, with average melting temperatures of 5°C and 9°C, respectively.

The objective of this study is to select the most suitable PCM for the required product temperature, and analyse its main effects on system performance, in order to improve PV sub-system integration. Specifically, a parametric study was performed, in order to evaluate the influence of TES slab thickness, insulation thickness, and compressor velocity on system performance. The revised output variables included product temperature, TES temperature, PV field size, and battery size.

doi:10.18086/eurosun2018.04.23 Available at http://proceedings.ises.org

Nomenclature

h	Specific enthalpy [kJ kg^{-1}]
q	Heat flow rate [W]
T	Temperature [K]
W	Electrical power [W]
V	Voltage [V]
I	Current [A]
R	Resistance [Ohm]
x	Space dimension [m]
t	Time [s]
k	Thermal conductivity [W m^{-1} K^{-1}]
p	Density [kg/m^3]
a	Parameter "a" of photovoltaic model [-]
C	Coefficient polynomial compressor curves
COP	Coefficient of Operation [-]

Subscripts

air	Air
com	Compressor
Int	Internal equipment
Inf	Infiltration
los	Losses
PCM	Phase change material
TES	Thermal energy storage
pr	Product
D	Diode
S	Series
P	Parallel
h	Horizontal
v	Vertical

2. System description and experimental setup

The analysed system (Fig. 1) consists of a horizontal direct current refrigerator, driven by electricity produced by a photovoltaic (PV) sub-system. The refrigeration cell has an upper door with a useful area of 0.59 m^2, and a volume capacity of 350L. The refrigeration sub-system is equipped with a direct current compressor (Danfoss, Secop, 35BD), an evaporator wall, and a natural air-cooled condenser. This sub-system uses a simple vapour compression refrigeration cycle with refrigerant R134a.

Electricity required by the refrigeration subsystem is produced in a PV sub-system, with multi-crystalline silicon modules (Peak power of 100W). In this sub-system, the energy is stored in electric lead acid batteries, and the charger controller permits to take the electricity from battery or directly from PV modules according to the system conditions.

The TES slab was located in contact with the evaporator wall, covering all internal walls of refrigeration cell. When the compressor starts (ON), the TES slab and the stored product start to be cooled. Once the product reaches the required set temperature, the compressor stops (OFF). In this way, during the compressor ON time, the TES slab is charged and stores cold thermal energy (sensible and latent). After this, during the compressor OFF time, the TES slab is discharged and contributes to remove heat from the stored product.

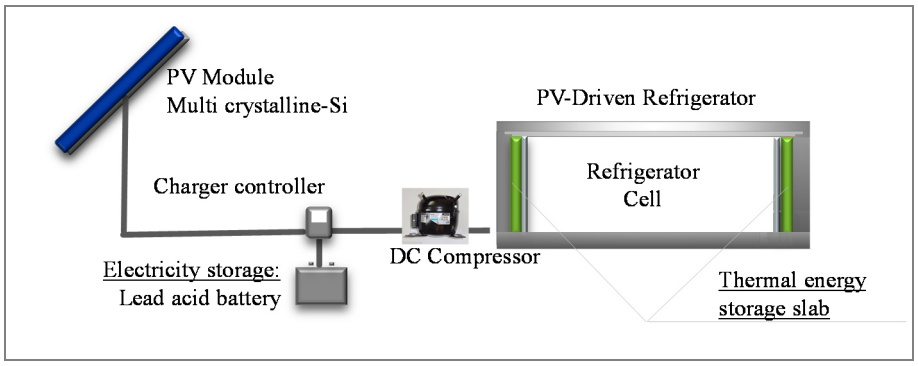

Fig. 1: System scheme

The system was modelled and simulated with three materials, with different average melting temperatures (0°C, 5°C and 9°C). In order to validate the model, the refrigeration cell was tested at the laboratory in a climatic room for 2 scenarios: 1) Refrigerator without TES and 2) Refrigerator with TES. The material used for TES during the test was RT5HC, manufactured by Rubitherm with average melting temperature of 5°C

Fig. 2 shows the main elements included in the experimental setup: the direct current refrigerator (a); the climatic room, in which the temperature and humidity were controlled by an air conditioning system (b); steel sheets with encapsulated PCM, to install in contact to evaporator-wall of the refrigerator (c), a standard electrical panel, used for supplying AC electricity (d), a regulated direct current source which converts AC to CC and provides electricity at 12V to the compressor (e), a data acquisition system (f), a hall sensor for measuring the CC current and complementary elements (g). The measurements were carried out according to the European Norm EN 62552 (IEC, 2013). More details in relation to the experimental setup were reported in a previous study (Coca-Ortegón et al., 2017).

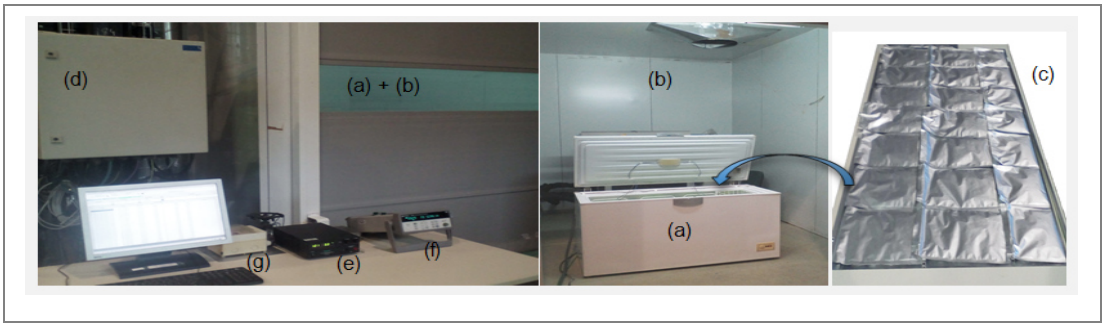

Fig. 2: Main elements of the experimental setup: (a) Refrigerator, (b) Climatic Room, (c) Encapsulated PCM in steel sheets, (d) AC Electrical panel, (e) DC source, (f). Data acquisition system, (g) Current sensors

3. Modelling and simulation

The general model was implemented in Matlab, and as a complementary tool was used the dynamic simulation software TRNSYS, in order to simulate the PV sub-system. The model includes four main blocks: the refrigerated cell or cabin (a), the energy thermal storage (TES) (b), the refrigeration sub-system (c), and the photovoltaic sub-system (d), with electrical storage using lead-acid batteries (See Fig.3).

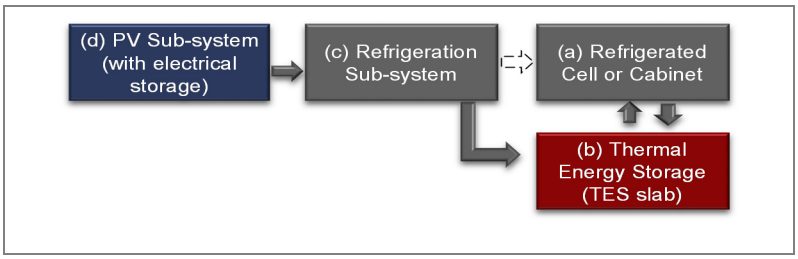

Fig. 3: Main blocks of developed model

The simulation was carried out for three different materials in the TES slab; Table 2 presents the main characteristics of them. The first material is distilled water; which was included in the study due to the low cost and the high sensible thermal storage capacity. The second and third materials are PCMs, which can store sensible and latent thermal energy. These PCMs are organic materials (paraffin's), manufactured by Rubitherm (references RT-5HC and RT-9). The main advantage of paraffin's is that they do not need to be sub-cooled for getting the crystallization, as occurs with water and hydrated salts.

Tab. 1: Main characteristics of phase change materials used in the simulation

Material	Units	Distilled Water	Rubitherm RT5HC	Rubitherm RT9
Class	-	Inorganic	Organic	Organic
Subclass	-	-	Paraffin	Paraffin
Phase change temperature	[°C]	0	4 to 6	7 to 11
Heat storage capacity	[kJ/kg]	334	250	175
Specific heat capacity (solid)	[kJ kg^{-1} K^{-1}]	2.09	2.0	2.0
Specific heat capacity (liquid)	[kJ kg^{-1} K^{-1}]	4.18	2.0	2.0
Density (solid)[1]	[kg m^{-3}]	900	880	880
Density (liquid)[2]	[kg m^{-3}]	1000	760	760
Thermal conductivity (solid)	[W m^{-1} K^{-1}]	1.8	0.2	0.2
Thermal conductivity (liquid)	[W m^{-1} K^{-1}]	0.4	0.2	0.2

[1] Value at -15°C. [2] Value at 20°C

3.1 Heat transfer in the PCM

As previously mentioned, the TES slab is arranged in contact to the evaporator wall (Fig 4). In this way, when the stored product needs to be cooled, the removed heat is transferred first from stored product to the air inside of refrigerator, second from air to the TES slab, and third, from the TES slab to the evaporator-wall.

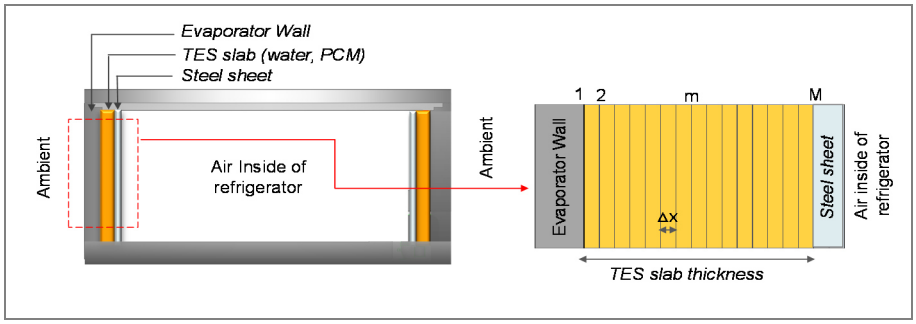

Fig. 4: Layout of the TES slab in the refrigerated cell and scheme of spatial discretization

For the analysed product temperature (11°C), "Water" is a particular case of PCM in which the process of phase change does not occur. Therefore, to model the TES slab with water, it is possible to apply the same procedure described for the heat transfer for the PCM slab described below.

Heat transfer in the PCM can be modelled, with a good accuracy, by a one-dimensional model, applying either the moving boundary method, developed by Stefan or the enthalpy method. Stefan's method (Fleischer, 2015) assumes that the PCM has a single phase change temperature, as occurs with pure crystalline and eutectic substances, while the enthalpy method (Ozisik, 1993) is suitable for PCMs that have a temperature region for the change phase process, as it happens with fatty substance and alloys.

In this study we used the enthalpy method, because the PCMs selected for the study are not pure substances and do not have a single phase change temperature. In this case, heat transfer in the PCM internal nodes is governed by the general 1-dimensional heat transfer equation (eq. 1), in which the PCM Temperature (T_{PCM}) and the PCM specific enthalpy (h_{PCM}) vary in the spatial dimension (x) and in the time dimension (t). In this equation the PCM thermal conductivity (k_{PCM}) and density (p_{PCM}) are considered constant in the liquid phase and in the solid phase, while in the phase change region, these properties are calculated by interpolation as previous studies indicate (Ozisik, 1993).

$$\frac{\partial}{\partial x} k_{PCM} \cdot \frac{\partial T_{PCM}}{\partial \mathrm{x}} = \rho_{PCM} \cdot \frac{\partial h_{PCM}}{\partial \mathrm{t}} \qquad \text{(eq.1)}$$

To solve the differential equation, we used the finite difference method. In this method, equation 1 was discretized, dividing the TES slab in the spatial dimension, with a Δx of 1mm, and an appropriate Δt value, in order to maintain the convergence conditions. Fig. 4 shows a scheme of the spatial division of the TES slab, in which the node "1" is in contact with the internal evaporator-wall, while the node "M" is in contact with the steel sheet arranged between the TES slab and the air inside of refrigerator. The system equations obtained after the discretization, were solved by applying the explicit method (Bergman et al., 2011; Patankar, 1980)

3.2 Refrigerated cell

Average temperature inside the refrigerated cell was calculated through energy balance equation (eq. 2), which takes into account the thermal load components, as well as the heat transfer rate between the TES slab and the air inside of refrigeration cell ($q_{TES\text{-}air}$)

$$q_{TES-air} = q_{los} + q_{pr} + q_{Int} + q_{Inf} \qquad \text{(eq.2)}$$

The thermal load components were calculated according to ASHRAE standards. These components include: Transmission heat gains or losses through the refrigerator enclosures (q_{los}), Product thermal load (q_{Pr}), heat gains due to internal equipment (q_{Int}), and infiltration heat gains (q_{Inf}). (ASHRAE, 2010).

In relation to transmission heat gains, the model considers the transmission heat gains through the vertical enclosures ($q_{los,v}$), which were taken into account in the boundary conditions at the external node of PCM , as well the transmission heat gains through the horizontal enclosures ($q_{los,h}$), which were included in the energy balance of the refrigerated cell.

3.3 Refrigeration sub-system

Refrigeration sub-system model is based on a simple mechanical compression refrigeration cycle, which uses R134a as refrigerant. The refrigerator has an evaporator-wall, made of a copper tube circuit, with external diameter of 7.92 mm; the heat transfer mode is forced convection. The condenser is wire on tube type, made of copper with external diameters of 4.75 and 1 mm for tubes and wires respectively, and dissipates the heat by natural convection. The compressor is alternative hermetic type, manufactured by Danfoss-Secop, BD35F. Table 2 presents the main characteristics of these components.

Tab.2: Main characteristics of refrigeration sub-system components

Element	Characteristics
Cell or cabinet	- Length x Width x Depth: 1.36x0.44x0.63 m^3 - Net Volume: 0.350 m^3
Compressor	- Type: Reciprocating, hermetic - Manufacturer: Danfoss, Model:BD35F, Voltage 12V DC - Refrigerant: R134a, Swept volume: 2 cm^3
Evaporator	- Heat transfer mode: Forced convection (adapted) - Type: Evaporator-wall, area: 2.033 m^2 - Tube: External diameter tube 7.92 mm, thickness 0.813mm, length 30.29m
Condenser	- Heat transfer mode: Natural convection - Type: Wire on tub (Cooper). - Tube: External diameter 4.75 mm, thickness 0.762mm, length 13.90 m -Wire: External diameter 1mm, length tube 106.6 m
Expansion element	- Type: Capillary tube - External diameter: 1 mm (Cooper)

The simulation of this refrigeration sub-system is based on the performance curves of the compressor, provided by the manufacturer, according to the European Norm EN-12900 (AENOR, 2014). This standard characterizes compressors performance through cubic regression curves, in which the cooling capacity (q_{com}) and the electrical power consumption (W_{com}) are expressed as a function of the evaporation (T_e) and condensation (T_c) temperatures, according to the following equation.

$$Y_{=}C_1 + C_2.T_e + C_3.T_c + C_4.T_e^2 + C_5.T_e.T_c + C_6.T_c^2 + C_7.T_c^3 + C_8.T_eT_c^2 + C_9.T_eT_c^2 + C_{10}.T_c^3 \qquad \text{(eq.3)}$$

The coefficients of the polynomial curves corresponding to the compressor used in the refrigeration sub-system were provided by the manufacturer, using the software Coolselector®2.

3.4 Photovoltaic sub-system

The dynamic simulation software Trnsys was used for simulating the PV sub-system; the components used in this simulation were: type 194 for the PV module, type 47a for electrical batteries, type 48b for the regulator, type 14h for power load profiles, and type 15.3 for the weather file.

In particular, the simulation of the photovoltaic module was based on the well-known “five parameters model”, whose equivalent circuit is shown in Fig. 5. This circuit is integrated by a direct current source, which simulates the photovoltaic production, a diode connected in parallel, which represents the semiconductor material of the photovoltaic cells, a resistor connected in series and a resistor connected in parallel (De Soto et al., 2006; Duffie and Beckman, 2013; Eckstein, 1990; Surith et al., 2013).

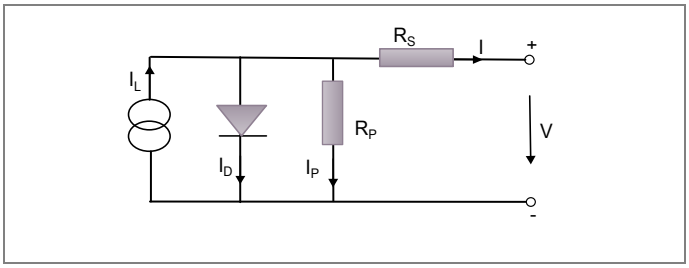

Fig. 5: Equivalent circuit model of 5 parameters photovoltaic module

The relation between the voltage (V) and the intensity (I) of the current supplied by the photovoltaic module is expressed by equation 4, in which it is necessary to know the five parameters of the model: the light current (I_L), the inverse saturation current of the diode (I_D), the series resistance (R_S), Parallel Resistance (R_P), and the "a" factor (De Soto et al., 2006). These parameters are calculated for reference conditions, using the manufacturer's datasheet.

$$I = I_L - I_D.\left(e^{\frac{V+I.R_S}{a}} - 1\right) - \frac{V + I.R_S}{R_P} \qquad \text{(eq.4)}$$

3.5 Base simulation conditions and performance indicators

The simulation was performed under the following base simulation conditions: ambient temperature at 25 ° C, since the refrigerator will be installed in a conditioned process area; product set temperature at 11 ± 2 ° C, insulation of polyurethane with a thickness of 80mm, compressor velocity of 3000 Rpm, internal air speed of 0.2 m/s, and air renewal rate of 0.25/h.

As case studied we selected a ripening cheese at 11°C for a small scale cheese processing process. Other application at this temperature can be some fruits and vegetables. The application was evaluated for the implementation in the region of Nyanza (Kenya).

A parametric analysis was carried out by varying the values of TES slab thickness, insulation thickness and compressor velocity. The revised output variables were the product temperature evolution, the TES materials temperature evolution, PV field size and the battery size. The battery was sized for a total autonomy time of the refrigerator without electricity supply of 24 h.

As performance indicators we used the compressor cycle time, the daily electricity consumption, and the mismatch between electricity production and power loads.

4. Results and Discussion

The simulation was carried out under the base conditions previously described. The analysis includes three materials: The first material was distilled water, which only store sensible thermal energy, and the others were PCMs (RT5HC and RT9) with average phase change temperatures of 5°C and 9° respectively, which store latent and sensible thermal energy. Detailed properties of these materials were already presented in Table 2.

The influence of the TES on the system, first considers effects of TES slab thickness variation, making simulations with thickness values between 5 and 12 mm. According to the results, the most suitable material was selected for the simulation base conditions.

Subsequently the influence of other two variables was considered: insulation thickness and compressor velocity. For these variables additional simulations were carried out, with insulation thickness values between 40 and 120 mm, and compressor velocity values of 2000, 2500, 3000 and 3500 min^{-1}.

Taking into account the relevance of the TES slab thickness, this study presents a more detailed analysis for this variable. In this case, we revise the TES slab thickness effects on the product temperature, TES materials temperature, electricity consumption, compressor cycle time, photovoltaic field size and the electrical battery size. For the other variables the analysis is centred only in the compressor cycle time, and the battery size.

4.1 Temperature evolution for stored product and studied materials

The evolution of product temperature in the refrigerator "Without TES" and refrigerator With TES, using different materials (water, RT5HC and RT9) are presented in Fig. 6, under simulation base conditions, with a TES slab thickness of 8mm and a product set-point temperature of 11± 2°C. The duration of analysed period was 48 hours.

During the maintenance cycles, the refrigerator "Without TES" maintains the product temperature between the required values (9 to 13°C). When the TES slab is installed, the maximum product temperature remains at the desired value (13°); however, the minimum product temperature drops slightly 1.4°C, 2.2°C, and 1.8°C below to the desired value (9°C), for water, RT5HC and RT9 respectively.

This is because the TES slab is charged when the compressor is ON and discharged while the compressor is OFF, removing additional heat from the product during the OFF time. This behaviour must be taken into account in the final control strategy definition, since it is necessary to control the allowed product sub-cooling

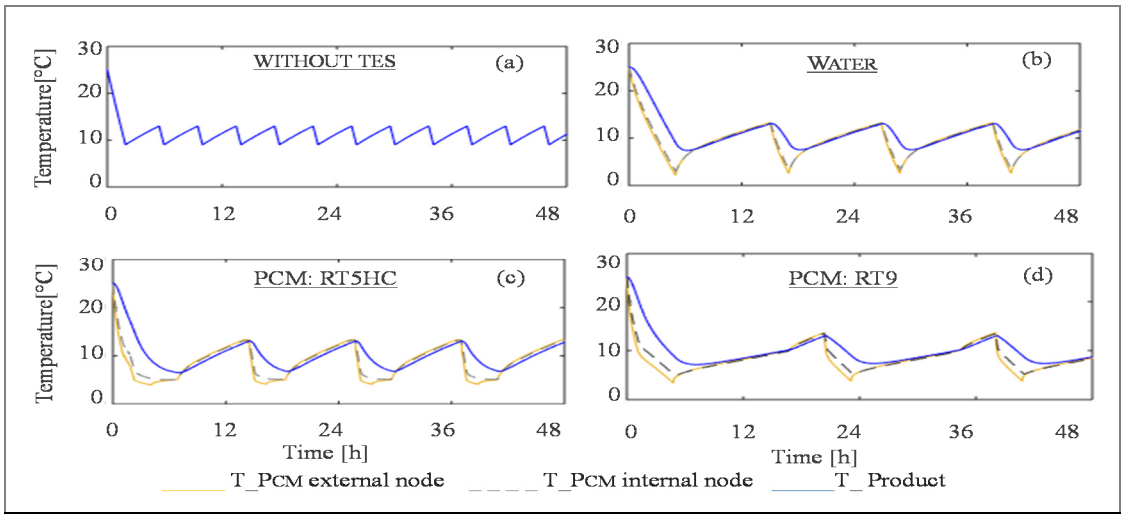

Fig. 6: Product and TES materials temperature evolution under simulation base conditions with a TES Slab thickness of 8mm

Fig. 6 also shows the TES materials temperature evolution, including the external node of the TES slab which is in contact with the evaporator-wall, as well as the internal node, which is closer to the indoor air of the refrigerated cell.

For Water, the minimum temperatures were 2.5°C and 3.4°C, at the external and internal nodes respectively; therefore, as it is expected, this material only store sensible thermal energy.

For the PCM RT5HC, the minimum temperatures were 4.2°C and 5.1°C at the external and internal node respectively. Since in this PCM, the phase change process was not completed, because the melting temperature region is between 4°C and 6°C; so this PCM took advantage from the latent thermal storage in a partial way.

For the PCM RT9, the minimum temperatures were 3.4°C at the external node, and 4.9°C at the internal node. In this case, the phase change process was completed because the melting temperature range is between 7°C and 10°C; therefore it was possible to take full advantage from the latent thermal storage.

These results indicate that the phase change process takes place in a complete way, when the phase change temperature of the PCM is closer to the set-temperature in the inside of the refrigerator, for the analysed case.

4.2 Effect of TES slab thickness on the compressor cycle time

Incorporation of a TES slab gives more inertia to the refrigerator and reduce the total number of compressor cycles. A compressor cycle include two parts, one in which the compressor is ON and the other in which the compressor is OFF.

For a better integration of the refrigerator with the PV sub-system, the number of compressor cycles per day should be near to one; that implies a minimum duration cycle of 24 hours. In this way it is easier to supply the electricity required by the system during the day, attend the thermal demand, and charge the TES slab. Later, during the night, the TES slab can be discharged and attend thermal demand without any electricity supply.

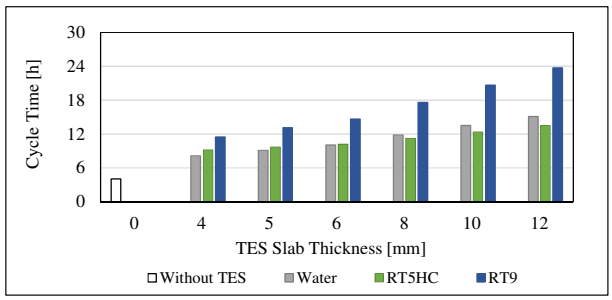

Fig. 7: Cycle time for different TES slab thickness

Taking into account the importance of the cycle duration, we simulated the system for several TES slab thickness values, and calculated the cycle duration time for the three analysed materials. Results under base simulation conditions, are presented in Fig.7. When the refrigerator does not have a TES slab, the cycle time is only 4.03 h.

If the TES slab thickness is about 4 mm, the cycle time increases to 8.1, 9.2 and 11.5h for water, the PCM RT5HC y the PCM RT9 respectively. If the slab thickness is 12 mm this cycle time increases to 15.1, 13.5, y 23.7 h for the same PCMs. These results indicate that the PCM RT9 is the most suitable for the analysed application because the longer cycle time, makes easier the integration of PV sub-system.

4.3 Effect of TES slab thickness on the electricity consumption

Despite the fact the TES slab gives more inertia to the system and improves the integration with the PV sub-system, the results show that the electricity consumed by the system also increases. Fig. 8 shows the electrical consumption for different TES slab thickness, under simulation base conditions and assuming that only maintenance cycles take place during the system operation.

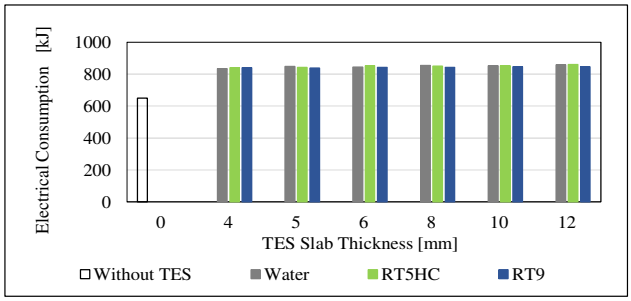

Fig. 8: Daily electricity consumption for different PCM slab thickness

When the refrigerator does not have TES, the daily electricity consumption is 649 kJ. There is an important variation when the refrigerator has a TES Slab, with increments between 28.5% and 32.1% for Water, between 29.5% and 32.4% for the PCM RT5HC, and between 29.4% and 30.5% for the PCM RT9. We can see that the thicker TES slab, the more electricity consumption there is, and the PCM RT9 has lower increments.

Regarding to PV sub-system design, a higher consumption may imply an increment in the photovoltaic field size. On the other hand, the incorporation of the TES slab also increases the cycle time, thanks to this increment, it is possible to improve the use of solar resource and to reduce the electrical battery size.

Therefore, in the following items these two points are analysed, the size of the photovoltaic field, as well as the size of the electrical batteries, when the TES slab is installed in the refrigerator.

4.4 PV field size and mismatch between PV production and power load profiles

At the location of the analysed application (region of Nyanza, Kenya, with a latitude of 0.08°N, and longitude of 35.06°E), the minimum electricity production of the photovoltaic field takes place during November. Therefore, this month was taken as the reference period for the analysis.

Taking into account the daily electricity consumption of the system, as well as the power demand, it is possible to size the photovoltaic field. For both cases: Refrigerator without and with TES slab, the electricity required by the system can be supplied by a small multi-crystalline silicon module, with a peak power of 100W STC. During the analysed month, this PV module has an average daily production of 1533 kJ/day, with minimum and maximum values of 1215 and 1807 kJ/day, respectively.

As usually occurs in this type of systems, there is a mismatch between PV production and power load. Fig. 9 illustrates this mismatch for the refrigerator without TES, and the refrigerator with TES (PCM RT9). In general, the thicker TES slab, the lower the number of cycles are, and the smaller the mismatch between the PV production and the power load is.

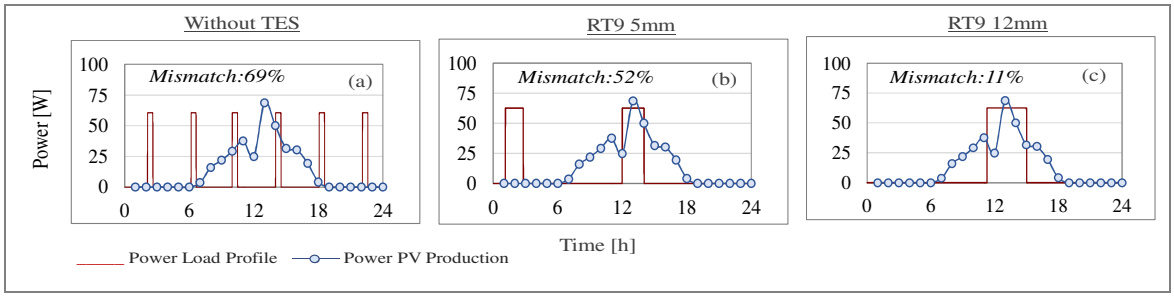

Fig. 9: Mismatch between Power PV Production and Power Load Profiles: (a) Refrigerator without TES (b) Refrigerator with PCM RT9 slab thickness of 5mm, (c) Refrigerator with PCM RT9 slab thickness of 12mm

Table 3 summarizes the mismatch obtained for the three materials considered in the study, with different TES slab thicknesses. The refrigerator without TES has an average mismatch of 72%; while the refrigerator with TES, this mismatch can be reduced up to 37%, 44% and 11% for water, the PCM RT5HC and the PCM RT9, respectively, when the TES slab thickness is 12mm.

Tab.3 Mismatch between power PV production and power load profiles for studied materials and different TES slab thickness

Material	TES Slab Thickness [mm]						
	0	4	5	6	8	10	12
Distilled Water	69%	57%	55%	55%	49%	44%	37%
RT5HC	69%	57%	55%	52%	48%	46%	44%
RT9	69%	55%	52%	46%	34%	21%	11%

4.5 Effect of TES slab thickness on the battery size

The electrical battery was sized taking into account the mismatch between the PV production and the power load profiles calculated previously. Other factors applied for battery sizing were the battery discharge efficiency (0.85) and the maximum depth of discharge (0.70). Fig. 10 shows the results under the simulation base conditions, for the three materials included in the analysis and different TES slab thickness.

The battery size for the refrigerator without TES is 209 Wh. The best results are obtained for the PCM RT9, in which the battery size is reduced to 44Wh (when the TES slab thickness is 12mm). For water and the PCM RT5HC the effects on the battery size are smaller, with final values of 148 and 175 Wh, respectively for the same simulation conditions. This results shows that the reduction of battery size can be between 16 and 78% according to the material selected for the TES Slab.

Better results of the PCM RT9 are mainly due to the fact this material has a complete phase change process,

and therefore it takes better advantage of the latent thermal energy storage, as was exposed in 4.1, in which the evolution of the temperature of the TES slabs was revised.

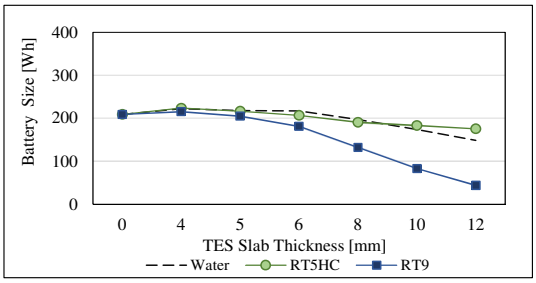

Fig. 10: Battery size for different PCM slab thickness

4.6 Effects of insulation thickness

Thermal loads due to transmission losses through the enclosures is highly important in the overall thermal load of the refrigerator. Therefore, insulation thickness has been widely analysed in numerous literature studies. ASHRAE recommends, among different types of insulation, polyurethane with a minimum thickness of 50 mm when the set product temperature is between 10 and 16 °C (ASHRAE, 2010).

Due to the importance of this variable, in this section we analysed the effects of insulation thickness on the duration of the compressor cycle, as well as on the electrical battery size. Since the most significant effects on the system were obtained for the PCM RT9, the simulations were performed with this material with TES slab thickness values of 8 and 10mm.

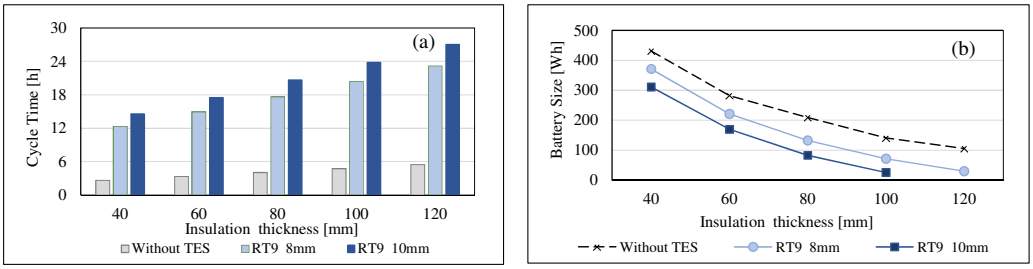

Fig. 11: Compressor cycle time and battery size for different insulation thickness

The refrigerator without TES, has a compressor cycle time between 2.6 and 5.4 hours, while in the refrigerator with the PCM RT9, the cycle time is closer to 24 hours, when insulation thickness is greater than 100mm (Fig 11 (a)). Through the combination of 100 mm of insulation thickness and a TES slab thickness of 10 mm, with the PCM RT9, this cycle time can increase up to 23.9 h.

Regarding the electrical battery size (Fig. 11 (b)), the effects are important in both cases: Refrigerator without TES and Refrigerator with TES. For the Refrigerator without TES, the electrical battery size has a reduction of 49%, when the insulation thickness changes from 80 to 120mm. On the other hand, for the Refrigerator with TES, with the PCM RT9, the electrical battery size can be reduced up to 78% when insulation thickness also changes from 80 to 120mm.

For the operation conditions analysed, the positive effects of increasing the insulation thickness on the size of the battery, are very important. This is because the transmission thermal losses represent 89% of the total thermal loads in the system. However, it is expected that at higher the internal thermal and infiltration loads, the PCMs will be more relevant.

4.7 Effects of compressor velocity

Table 4 summarizes the effects of the variation of compressor velocity on the system; these results are presented for a TES Slab thickness of 10mm and the PCM RT9. The faster compressor velocity, the shorter cycle time is, for instance, when the compressor velocity changes from 2000 to 3500 min^{-1}, the cycle time increases from

19.2 h to 21.0h. In addition, the "Time ON" for the compressor decreases from 4.4h to 2.9h, and this reduction has a positive effect on the compressor useful life.

Tab.4 Results for different compressor velocities for the PCM RT-9 with slab thickness of 10mm

Description	Units	Compressor Velocity (min^{-1})			
		2000	2500	3000	3500
Cycle Time	[h]	19.2	19.9	20.7	21.5
Time ON	[h]	4.4	3.7	3.2	2.9
Time OFF	[-]	14.8	16.2	17.4	18.5
Ratio Time ON / Time OFF	[-]	0.296	0.225	0.185	0.158
Average Power	[W]	36.7	48.3	58.6	68.9
Electricity consumption	[Wh/day]	223	231	235	239
COP System	[-]	3.42	3.24	3.17	3.12
Electrical batteries size	[Wh]	94	86	83	63

On the other hand, this increase of compressor velocity, also produces a slight increment of 7% in the daily electricity consumption, and a strong increment of 88% in the power demand. Despite this effect, it was found that PCM charging process is more effective, since there is a reduction of 33% for the electrical battery size. This means that the PCM takes more advantage from the thermal energy storage (sensitive and latent), when the compressor velocity is higher.

This performance must be taken into account in the definition of system control strategy. It is recommended to regulate the compressor at high velocity when the solar radiation is also high, and at low velocity when the solar radiation is also low.

5. Conclusions

A PV-refrigerator was modelled and simulated, under base operating conditions, at 11±2°C product temperature and 25°C ambient temperature. Three materials were included in the simulations: one was water, and the others were PCM with average phase change temperatures of 5°C and 9°C, respectively. The analysis considered the effects of three relevant variables: TES slab thickness, insulation thickness, and compressor velocity.

The thicker the TES slab, the longer the cycle duration is. For improving PV sub-system integration, compressor cycle time had to be a minimum of 24 hours. In this regard, longer cycle times were obtained for the PCM whose average phase change temperature was 9°C, with slab thickness greater than 8mm.

On the other hand, the TES slab installed in contact with the evaporator-wall, in the internal side of the refrigerator, increased the daily electricity consumption. In light of this, the effects on PV field size and electrical battery size in the analysed operation conditions should be evaluated.

In the present study, the final selected PV module had 100W of peak power, under standard test conditions. The electricity required by the system provided for this PV module in both cases: Refrigerator without TES and the Refrigerator with TES. In regards to electrical battery size, the best results are obtained with the PCM RT9, manufactured by Rubitherm, as this material took more advantage of latent storage, in comparison to the other analysed materials.

Insulation thickness also influenced system performance. Under the operation conditions analysed, this impact was especially important because almost the entirety of the thermal load was due to transmission losses through refrigerator enclosures. However, this impact may be lower when the internal and infiltration thermal loads increase, and in that case TES with PCM will get more relevant.

A higher compressor velocity helped to reduce the electrical batteries size, but it did increase the power demand. This behaviour must be taken in to account, in order to define a system control strategy. It is it is recommended that the compressor operates at higher velocity when solar irradiation is high, and at lower velocity when solar irradiation is low.

6. Acknowledgement

The authors are grateful to URV-Solidaria, and AGAUR (FI-DGR 2017), program co-financed by the European Social Funds.

7. References

AENOR, 2014. UNE-EN 12900. Refrigerant compressors. Rating conditions, tolerances and presentation of manufacturer's performance data. doi:M 27527:2014

ASHRAE, 2010. Handbook of Refrigeration. American Society of Heating, Refrigerating and Air-Conditioning Engineers (ASHRAE), Atlanta (US).

Azzouz, K., Leducq, D., Gobin, D., 2009. Enhancing the performance of household refrigerators with latent heat storage: An experimental investigation. Int. J. Refrig. 32, 1634–1644. doi:10.1016/j.ijrefrig.2009.03.012

Bergman, T.L., Lavine, A.S., Incropera, F.P., DeWitt, D.P., 2011. Introduction to heat transfer, Sixth Edit. ed. John Wiley & Sons, US.

Cheng, W. long, Ding, M., Yuan, X. dong, Han, B.C., 2017. Analysis of energy saving performance for household refrigerator with thermal storage of condenser and evaporator. Energy Convers. Manag. 132, 180–188. doi:10.1016/j.enconman.2016.11.029

Coca-Ortegón, A., Torres-Toledo, V., Müller, J., Coronas, A., 2017. Assessment of a Solar Powered Refrigerator Equipped with Thermal Storage for a Dairy Application. Proc. SWC2017/SHC2017 1–12. doi:10.18086/swc.2017.28.02

De Soto, W., Klein, S.A., Beckman, W.A., 2006. Improvement and validation of a model for photovoltaic array performance. Sol. Energy 80, 78–88. doi:10.1016/j.solener.2005.06.010

Duffie, J., Beckman, W., 2013. Solar engineering of thermal processes, 4th Editio. ed. John Wiley & Sons, Wisconsin-Madison.

Eckstein, J.H., 1990. Detailed modelling of photovoltaic system components. University of Wisconsin - Madison.

Fleischer, A.S., 2015. Thermal energy storage using phase change materials. Fundamentals and applications. Springer, US. doi:10.1007/978-3-319-20922-7

IEC, 2013. EN 62552 Household refrigerating appliances - Characteristics and test methods.

Marques, A.C., Davies, G.F., Maidment, G.G., Evans, J. a., Wood, I.D., 2014. Novel design and performance enhancement of domestic refrigerators with thermal storage. Appl. Therm. Eng. 63, 511–519. doi:10.1016/j.applthermaleng.2013.11.043

Oró, E., De Gracia, A., Castell, A., Farid, M.M., Cabeza, L.F., 2012. Review on phase change materials (PCMs) for cold thermal energy storage applications. Appl. Energy 99, 513–533. doi:10.1016/j.apenergy.2012.03.058

Ozisik, M.N., 1993. Heat Conduction, Second Edi. ed. John Wiley & Sons, Inc., New York. doi:10.1002/9781118411285

Patankar, S., 1980. Numerical Heat Transfer and Fluid Flow. Ser. coputational methods Mech. Therm. Sci.

Pedersen, H., Katic, I., 2016. Direct drive solar coolers, in: 12th IIR Gustav Lorentzen Natural Working Fluids Conference. Papaer ID 1070. Edinburgh, p. 8. doi:10.18462/iir.gl.2016.1070

Schaddelee-Scholten, B., Tempowski, J., 2017. Recycling used Lead-Acid Batteries: health considerations, 1st ed. World Health Organization, Geneve (Switzerland).

Sørensen, B., 2015. Chapter 11 - Environmental Issues Associated with Solar Electric and Thermal Systems with Storage, in: Sørensen, B. (Ed.), Solar Energy Storage. Elsevier Inc /Academic Press, United Kingdom, pp. 247–271. doi:10.1016/B978-0-12-409540-3.00011-6

Surith, N., Vishnu, V., Raam, K., Sai, P., Ramya, K., 2013. Photovoltaic Driven Dual Purpose Thermoelectric Refrigerator for Rural India. Int. J. Adv. Res. Technol. 2, 111–117.